Magnetic transitions and superconductivity in the *t-J* model

A. Sherman
Institute of Physics, Riia 142, EE-2400 Tartu, Estonia
(Received 23 April 1996; revised manuscript received 19 August 1996)

With the use of the spin-wave and Born approximations the energy spectrum of the two-dimensional *t-J* model is self-consistently calculated in the range of hole concentrations, $0 \leqslant x \lesssim 0.3$. The anomalous magnon Green's functions, which arise due to the hole-magnon interaction, are taken into consideration. They lead to a sharp transition from short-range antiferromagnetic order to a completely disordered paramagnetic state at $x \approx 0.19$, in addition to the transition from long-range to short-range antiferromagnetic order at $x \approx 0.02-0.04$. In the region of hole concentrations $0.04 \lesssim x \lesssim 0.19$ the obtained shape of the Fermi surface, the hole dispersion near the Fermi level, and the density of states on it are in satisfactory agreement with experiment in $La_{2-x}Sr_xCuO_4$ and Bi2212. The Eliashberg formalism is used for calculating T_c. The hole-magnon interaction is found to be unable alone to give rise to superconductivity. By adding a moderate interaction with apex oxygen vibrations high T_c's are obtained for even-frequency $d_{x^2-y^2}$ pairing in the range $0.04 \lesssim x \lesssim 0.19$. For larger hole concentrations the odd-frequency *s*-wave solution becomes the leading one which can lead to *s*-wave superconductivity in the overdoped regime with the participation of a hole-phonon interaction of the respective symmetry. [S0163-1829(97)06101-8]

I. INTRODUCTION

Strong electron correlations play a great role in unusual normal-state and superconducting properties of cuprate perovskites. In particular, extended van Hove singularities,[1] which are considered to be responsible for a part of these properties,[2] are supposed to be connected with the correlations. Their microscopic description is usually based on the extended Hubbard model or the related *t-J* model. The aim of the present paper is to consider the energy spectrum of the *t-J* model with special emphasis on the changes in magnetic ordering with hole concentration x. The region of small and intermediate concentrations was considered in Refs. 3–5. It was shown that in agreement with experiment[6] the two-dimensional (2D) *t-J* model was able to describe the transition from long-range to short-range antiferromagnetic ordering at $x \approx 0.02-0.04$ and the existence of large flat regions on the energy band near the Fermi level around the points $\mathbf{k}=(\pm\pi,0),(0,\pm\pi)$ at moderate x. By the position and extension these flat regions are completely analogous to the extended saddle points of the photoemission experiments.[1] Also the obtained Fermi surfaces appear to be close to those observed in these experiments.

The anomalous magnon Green's functions, which arise due to the hole-magnon interaction, are small for small x and therefore they were omitted in our previous consideration. The respective terms are included in the present calculations where, as in Refs. 4 and 5, the spin-wave[7,8] and Born approximations are used. The anomalous magnon Green's functions are found to lead to some quantitative changes for moderate x. However, the most essential, qualitative changes occur in the overdoped region where due to these terms at $x \approx 0.19$ the system exhibits a second transition, this time from short-range order to a completely disordered paramagnetic state. The analogy can be drawn with the result of neutron scattering experiments on $YBa_2Cu_3O_{7-y}$ where the disappearance of antiferromagnetic fluctuations in the normal state of overdoped samples was detected.[9] Another possible consequence of this transition is the change of the symmetry of the superconducting order parameter. For small and intermediate values of x the hole-magnon interaction was found to be unable alone to give rise to superconductivity. By adding a moderate interaction with apex oxygen vibrations high T_c's are obtained for $d_{x^2-y^2}$ pairing.[5] This symmetry of the order parameter was found in the major part of theories taking into account antiferromagnetic ordering and the hole-magnon interaction as the main mechanism of pairing.[10] It is clear that with the destruction of short-range antiferromagnetic order the situation is dramatically changed and the *s*-wave superconductivity, as in conventional superconductors, has to become dominating. Indeed, we found a sharp growth of odd-frequency *s*-wave superconducting fluctuations near the paramagnetic transition where the $d_{x^2-y^2}$-wave fluctuations disappear rapidly.

The outline of the paper is as follows. In Sec. II we formulate the theoretical model and derive the self-energy equations. The calculation procedure is discussed in Sec. III. The energy spectrum and manifestations of magnetic transitions in it are considered in Sec. IV. The Eliashberg equation and its solutions for different symmetries of the order parameter are discussed in Sec. V.

II. SELF-ENERGY EQUATIONS

The 2D *t-J* model, used as the basis of our model, has been shown[11,12] to be a good approximation for the low-energy dynamics of the Emery model,[13] which gives a realistic description of CuO_2 planes of cuprate perovskites. In the spin-wave approximation, the *t-J* Hamiltonian can be written in the form[7,8,12]

$$H=\sqrt{2}\sum_{\mathbf{k}\mathbf{k}'\sigma}(g_{\mathbf{k}\mathbf{k}'}h^{\dagger}_{\mathbf{k}\sigma}h_{\mathbf{k}-\mathbf{k}',-\sigma}b_{\mathbf{k}'\sigma}+\text{H.c.})+\sum_{\mathbf{k}\sigma}\omega^{0}_{\mathbf{k}}b^{\dagger}_{\mathbf{k}\sigma}b_{\mathbf{k}\sigma}$$
$$-\frac{4\varepsilon}{N}\sum_{\mathbf{k}\mathbf{k}'\mathbf{q}\sigma}\gamma_{\mathbf{q}}h^{\dagger}_{\mathbf{k}-\mathbf{q},\sigma}h_{\mathbf{k}\sigma}h^{\dagger}_{\mathbf{k}'+\mathbf{q},-\sigma}h_{\mathbf{k}',-\sigma}, \quad (1)$$

where $h^{\dagger}_{\mathbf{k}\sigma}$ is the creation operator of a hole with the 2D wave vector $\mathbf{k}$ in one of the classical Néel states, $\sigma=\pm1$ labels two sublattices with spins up or down in this state, and summations over $\mathbf{k}$ are limited to the magnetic Brillouin zone. $b^{\dagger}_{\mathbf{k}}$ is the creation operator of a magnon with the unperturbed frequency $\omega^{0}_{\mathbf{k}}=2J\sqrt{1-\gamma^{2}_{\mathbf{k}}}$, where J is the superexchange constant, $\gamma_{\mathbf{k}}=[\cos(k_x)+\cos(k_y)]/2$. The interaction constant $g_{\mathbf{k}\mathbf{k}'}=-4t(\gamma_{\mathbf{k}-\mathbf{k}'}u_{\mathbf{k}'}+\gamma_{\mathbf{k}}v_{\mathbf{k}'})/\sqrt{N}$ comprises the hopping constant t, the number of sites N, $u_{\mathbf{k}}=\cosh(\alpha_{\mathbf{k}})$, $v_{\mathbf{k}}=-\sinh(\alpha_{\mathbf{k}})$, and $\alpha_{\mathbf{k}}=\ln[(1+\gamma_{\mathbf{k}})/(1-\gamma_{\mathbf{k}})]/4$. The first term in Eq. (1) is the hole kinetic term. Its form reflects the fact that in the t-J model on the antiferromagnetic background the hole movement is accompanied by the emission and absorption of magnons. Their energy is described by the second term. The last term in Eq. (1) describes the static attraction of holes on neighboring sites due to the bond-breaking mechanism[14] with the binding energy ε.

Self-energy equations have been derived in the Born approximation. Its applicability is based on the small parameter x in the case of very small hole concentrations, when hole bandwidths are comparable with the limiting magnon frequency,[3] and on a small ratio of the magnon frequency to the hole bandwidth[15] for $x\gtrsim0.04$, when narrow spin-polaron bands are transformed into a much wider band with a bandwidth of the order of $t\gg J$.[4] The self-energy equation can be written in the form

$$G(\mathbf{k},i\omega_n)=[i\omega_n+\mu-\Sigma(\mathbf{k},i\omega_n)]^{-1},$$
$$\hat{D}(\mathbf{k},i\omega_\nu)=[i\omega_\nu\hat{\sigma}_3-\omega^{0}_{\mathbf{k}}\hat{\sigma}_0-\hat{\Pi}(\mathbf{k},i\omega_\nu)]^{-1},$$
$$\Sigma(\mathbf{k},i\omega_n)=-2T\sum_{\mathbf{k}'\nu}\{g_{\mathbf{k}\mathbf{k}'}g_{\mathbf{k}'-\mathbf{k},\mathbf{k}'}[D_{12}(\mathbf{k}',i\omega_\nu)+D_{21}(\mathbf{k}',i\omega_\nu)]+g^{2}_{\mathbf{k}\mathbf{k}'}D_{11}(\mathbf{k}',i\omega_\nu)+g^{2}_{\mathbf{k}'-\mathbf{k},\mathbf{k}'}D_{11}(-\mathbf{k}',-i\omega_\nu)\}\times G(\mathbf{k}-\mathbf{k}',i\omega_n-i\omega_\nu), \quad (2)$$
$$\Pi_{11}(\mathbf{k},i\omega_\nu)=\Pi_{22}(-\mathbf{k},-i\omega_\nu)=2T\sum_{\mathbf{k}'n}g^{2}_{\mathbf{k}'\mathbf{k}}G(\mathbf{k}',i\omega_n)G(\mathbf{k}'-\mathbf{k},i\omega_n-i\omega_\nu),$$
$$\Pi_{12}(\mathbf{k},i\omega_\nu)=\Pi_{21}(\mathbf{k},i\omega_\nu)=2T\sum_{\mathbf{k}'n}g_{\mathbf{k}'\mathbf{k}}g_{\mathbf{k}-\mathbf{k}',\mathbf{k}}G(\mathbf{k}',i\omega_n)\times G(\mathbf{k}'-\mathbf{k},i\omega_n-i\omega_\nu).$$

Here $G(\mathbf{k},i\omega_n)$ and $\hat{D}(\mathbf{k},i\omega_\nu)$ are the Fourier transforms of the Green's functions

$$G(\mathbf{k}\tau)=-\langle\mathcal{T}h_{\mathbf{k}\sigma}(\tau)h^{\dagger}_{\mathbf{k}\sigma}\rangle,\quad \hat{D}(\mathbf{k}\tau)=-\langle\mathcal{T}\hat{B}_{\mathbf{k}\sigma}(\tau)\hat{B}^{\dagger}_{\mathbf{k}\sigma}\rangle,$$

which, as follows from Eqs. (2), do not depend on the sublattice index σ. Angular brackets denote averaging over the grand canonical ensemble, $\mathcal{T}$ is the time-ordering operator, $h_{\mathbf{k}\sigma}(\tau)=\exp[(H-\mu\mathcal{N})\tau]h_{\mathbf{k}\sigma}\exp[-(H-\mu\mathcal{N})\tau]$ with the chemical potential μ, and the hole number operator $\mathcal{N}=\Sigma_{\mathbf{k}\sigma}h^{\dagger}_{\mathbf{k}\sigma}h_{\mathbf{k}\sigma}$. The hole-hole interaction adds the constant term $-4\varepsilon x$ to the hole self-energy. This term is included in the chemical potential. T is the temperature, ω_n and ω_ν are odd and even Matsubara frequencies, and $\hat{\sigma}_i$ are the Pauli matrices. In $\hat{D}(\mathbf{k}\tau)$, $\hat{B}^{\dagger}_{\mathbf{k}\sigma}$ is the two-component magnon operator $(b^{\dagger}_{\mathbf{k}\sigma},b_{-\mathbf{k},-\sigma})$. Thus, Eqs. (2) contain the anomalous magnon Green's functions

$$D_{12}(\mathbf{k}\tau)=-\langle\mathcal{T}b_{\mathbf{k}\sigma}(\tau)b_{-\mathbf{k},-\sigma}\rangle,\quad D_{21}(\mathbf{k}\tau)=-\langle\mathcal{T}b^{\dagger}_{-\mathbf{k},-\sigma}(\tau)b^{\dagger}_{\mathbf{k}\sigma}\rangle. \quad (3)$$

As follows from Eqs. (2), $\Pi_{12}(\mathbf{k},i\omega_\nu)$ and $\Pi_{11}(\mathbf{k},i\omega_\nu)$ have the same structure and can be of a comparable value. As a consequence, in the overdoped region the anomalous magnon Green's functions become comparable with $D_{11}(\mathbf{k},i\omega_\nu)$.

Self-energies in Eqs. (2) can be described by the following diagrams:

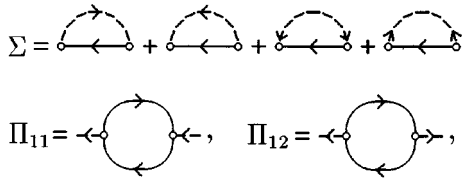

where solid and dashed lines correspond to hole and magnon Green's functions, respectively. A set of self-energy equations which is analogous to Eqs. (2) was obtained in Ref. 16.

Equations (2) are inconvenient for calculations due to reasons discussed in the next section. Instead we use the real frequency version of these equations. It can be obtained from Eqs. (2) by application of the spectral representations for Green's functions. First it should be verified that there exist such representations for functions (3),

$$D_{ij}(\mathbf{k},i\omega_\nu)=\int_{-\infty}^{\infty}\frac{d\omega}{\pi}\frac{B_{ij}(\mathbf{k}\omega)}{\omega-i\omega_\nu}, \quad (4)$$

where, as for $G(\mathbf{k},i\omega_n)$ and the diagonal elements of $\hat{D}(\mathbf{k},i\omega_\nu)$, the spectral functions $B_{ij}(\mathbf{k}\omega)$ are real. Taking into account that $G(\mathbf{k},i\omega_n)$ is invariant with respect to the transformations of the point group D_4 of the 2D lattice, it can be seen from Eqs. (2) that

$$\Pi^{*}_{22}(\mathbf{k},i\omega_\nu)=\Pi_{11}(\mathbf{k},i\omega_\nu),\quad \Pi^{*}_{12}(\mathbf{k},i\omega_\nu)=\Pi_{12}(\mathbf{k},i\omega_\nu),$$

and consequently

$$D^{*}_{12}(\mathbf{k},i\omega_\nu)=D_{12}(\mathbf{k},i\omega_\nu).$$

Since by definition

$$D_{21}(\mathbf{k},i\omega_\nu)=D^{*}_{12}(\mathbf{k},-i\omega_\nu)=D^{*}_{12}(-\mathbf{k},i\omega_\nu),$$

and $D_{ij}(\mathbf{k},i\omega_\nu)$ are also invariant with respect to the group transformations, we come to the conclusion that

$$D_{21}(\mathbf{k},i\omega_\nu)=D_{12}(\mathbf{k},i\omega_\nu).$$

This equality requires that the spectral functions

$$B^*_{21}(\mathbf{k}\omega)=B_{12}(\mathbf{k}\omega)$$

be real. It is now easy to verify that these functions are equal to the imaginary parts of the respective retarded Green's functions. Substituting the spectral representations analogous to Eq. (4) into Eqs. (2) and using the analytic continuation we find

$$G(\mathbf{k}\omega)=[\omega+\mu-\Sigma(\mathbf{k}\omega)]^{-1},$$

$$\begin{aligned}\mathrm{Im}\Sigma(\mathbf{k}\omega)=-2\sum_{\mathbf{k}'}\int_{-\infty}^{\infty}\frac{d\omega'}{\pi}\{&g^2_{\mathbf{k}\mathbf{k}'}\mathrm{Im}D_{11}(\mathbf{k}'\omega')\\&-g^2_{\mathbf{k}-\mathbf{k}',-\mathbf{k}'}\mathrm{Im}D_{11}(-\mathbf{k}',-\omega')\\&+2g_{\mathbf{k}\mathbf{k}'}g_{\mathbf{k}-\mathbf{k}',-\mathbf{k}'}\mathrm{Im}D_{12}(\mathbf{k}'\omega')\}\\&\times[n_B(\omega')+n_F(\omega'-\omega)]\\&\times\mathrm{Im}G(\mathbf{k}-\mathbf{k}',\omega-\omega'),\end{aligned}$$

$$D_{11}(\mathbf{k}\omega)=\frac{R^*(\mathbf{k},-\omega)}{R(\mathbf{k}\omega)R^*(\mathbf{k},-\omega)-\Pi^2_{12}(\mathbf{k},\omega)},$$

$$D_{12}(\mathbf{k}\omega)=\frac{\Pi_{12}(\mathbf{k},\omega)}{R(\mathbf{k}\omega)R^*(\mathbf{k},-\omega)-\Pi^2_{12}(\mathbf{k},\omega)},\qquad(5)$$

$$\begin{aligned}\mathrm{Im}\Pi_{11}(\mathbf{k}\omega)=2\sum_{\mathbf{k}'}g^2_{\mathbf{k}'\mathbf{k}}\int_{-\infty}^{\infty}\frac{d\omega'}{\pi}&\mathrm{Im}G(\mathbf{k}'\omega')\\&\times\mathrm{Im}G(\mathbf{k}'-\mathbf{k},\omega'-\omega)[n_F(\omega')\\&-n_F(\omega'-\omega)],\end{aligned}$$

$$\begin{aligned}\mathrm{Im}\Pi_{12}(\mathbf{k}\omega)=2\sum_{\mathbf{k}'}g_{\mathbf{k}'\mathbf{k}}g_{\mathbf{k}'-\mathbf{k},-\mathbf{k}}\int_{-\infty}^{\infty}\frac{d\omega'}{\pi}&\mathrm{Im}G(\mathbf{k}'\omega')\\&\times\mathrm{Im}G(\mathbf{k}'-\mathbf{k},\omega'-\omega)[n_F(\omega')\\&-n_F(\omega'-\omega)],\end{aligned}$$

$$\mathrm{Re}\Sigma(\mathbf{k}\omega)=\mathcal{P}\int_{-\infty}^{\infty}\frac{d\omega'}{\pi}\frac{\mathrm{Im}\Sigma(\mathbf{k}\omega')}{\omega'-\omega},$$

$$Re\Pi_{ij}(\mathbf{k}\omega)=\mathcal{P}\int_{-\infty}^{\infty}\frac{d\omega'}{\pi}\frac{\mathrm{Im}\Pi_{ij}(\mathbf{k}\omega')}{\omega'-\omega},$$

where $G(\mathbf{k}\omega)$ and $D_{ij}(\mathbf{k}\omega)$ are the retarded Green's functions, $R(\mathbf{k}\omega)=\omega-\omega^0_{\mathbf{k}}-\Pi_{11}(\mathbf{k}\omega)$, $n_B(\omega)=[\exp(\omega/T)-1]^{-1}$, and $n_F(\omega)=[\exp(\omega/T)+1]^{-1}$.

III. CALCULATION PROCEDURE

The following parameters were used in the calculations:

$$J=0.2t,\quad \varepsilon=0.5J.\qquad(6)$$

They were estimated with the use of the known parameters[17] of La_2CuO_4 and the mapping procedure of the extended Hubbard model onto the t-J model[12] (this procedure gives for J/t the range $0.1\lesssim J/t\lesssim 0.5$ from which the above value has been picked; the uncertainty is connected with the uncertainty in the parameters of La_2CuO_4 and with a possible influence of terms dropped from the extended Hubbard Hamiltonian). Since the parameters are related to well-isolated CuO_2 planes, they can be expected to be approximately valid also for related p-type cuprate perovskites. From these estimations $t\approx 0.5$eV. The ranges of the hole concentrations $0\leqslant x\lesssim 0.3$ and temperatures $0\leqslant T\leqslant 0.05t$ were considered.

Equations (5) were solved iteratively on a 20×20 lattice. Sets of equally spaced 400 points in the frequency range $-5t\leqslant\omega\leqslant 4t$ and 54 points with the same spacing in the range $-0.4t\leqslant\omega\leqslant 0.8t$ were used for the representation of the hole and magnon Green's functions, respectively. To make the iteration procedure stable the respective artificial broadenings $0.045t$ and $0.015t$ were introduced into these Green's functions. Simple iterations are well convergent only for small hole concentrations, while the chemical potential is widely spaced from the intensive quasiparticle peaks in the hole spectrum. The instability arising when μ approaches these peaks can be overcome as follows: Let $A^f(\mathbf{k}\omega)=\mathrm{Im}G^f(\mathbf{k}\omega)$ and $B^f_{ij}(\mathbf{k}\omega)=\mathrm{Im}D^f_{ij}(\mathbf{k}\omega)$ be the spectral functions obtained from some initial values $A^i(\mathbf{k}\omega)$ and $B^i_{ij}(\mathbf{k}\omega)$ in an iteration step; for the next step the linear combinations $(1-c)A^f(\mathbf{k}\omega)+cA^i(\mathbf{k}\omega)$ and $(1-c)B^f_{ij}(\mathbf{k}\omega)+cB^i_{ij}(\mathbf{k}\omega)$ are used as initial values. $c=0.7$ was enough to reach convergence in the major part of the considered concentration range. The larger value $c=0.9$ was necessary only near the transition from short-range order to the paramagnetic state. To verify convergence with the use of this procedure spectral functions obtained in widely separated iteration steps were compared.

An iteration procedure can be also applied for solving the imaginary frequency version of self-energy equations (2). We carried out such calculations and compared results with Matsubara Green's functions obtained from retarded Green's functions of Eqs. (5) and spectral representations (4). Perceptible differences between the two results were observed even at the imaginary frequency cutoff $\omega_c=30t$ which is more than 3 times larger than the considered real frequency range. The source of these differences can be understood from the equation

$$\begin{aligned}\Pi_{11}(\mathbf{k},i\omega_\nu)=2\sum_{\mathbf{k}'}g^2_{\mathbf{k}'\mathbf{k}}\int\int_{-\infty}^{\infty}\frac{d\omega_1 d\omega_2}{\pi^2}&\mathrm{Im}G(\mathbf{k}',\omega_1)\\&\times\mathrm{Im}G(\mathbf{k}'-\mathbf{k},\omega_2)T\\&\times\sum_n\frac{1}{(\omega_1-i\omega_n)(\omega_2-i\omega_n+i\omega_\nu)},\end{aligned}$$

which is derived from the respective equation (2) and spectral representations for the hole Green's function. As follows from Eqs. (5), in the real frequency version of the above equation the sum over n is substituted by the function $[n_F(\omega_1)-n_F(\omega_2)]/(\omega_1-\omega_2-i\omega_\nu)$. The introduction of the cutoff transforms this infinite sum into a finite one. However, the sum converges rather slowly to the function, especially for $|\omega_1|,|\omega_2|\gg T$. This is the reason for the mentioned differences in results of the two approaches. A further increase of the cutoff frequency in the imaginary frequency equations

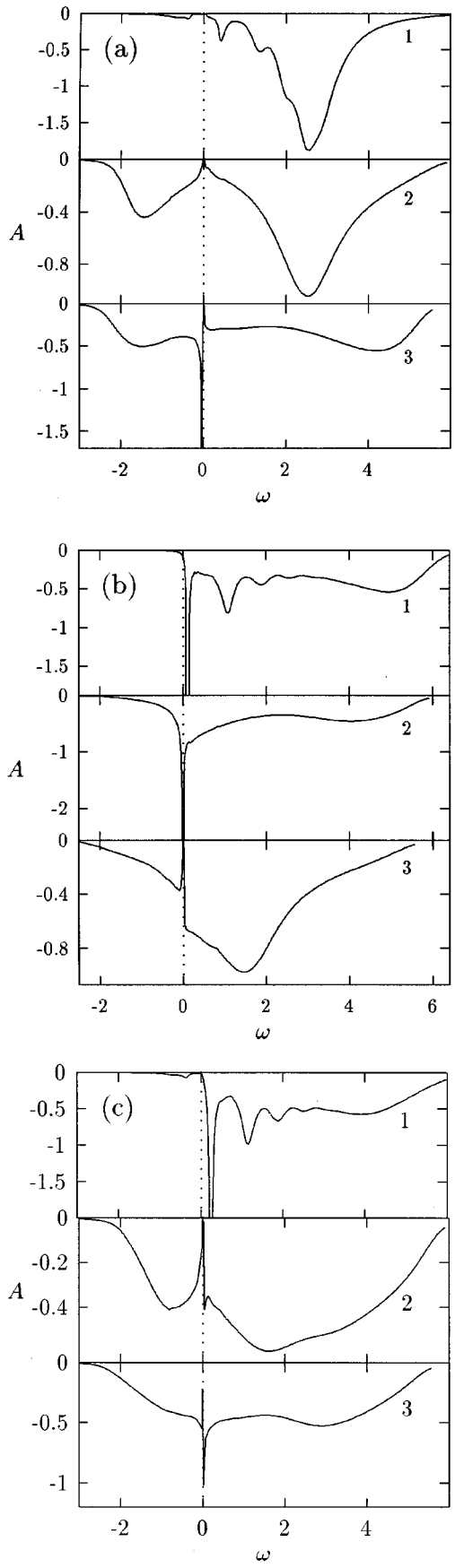

FIG. 1. The hole spectral function $A(\mathbf{k}\omega)$ for $\mathbf{k}=(0,0)$ (a), $(0,\pi)$ (b), and $(0,0.4\pi)$ (c). $T=0$. Curves 1, 2, and 3 correspond to $x=0.021$, 0.169, and 0.195, respectively.

imposes much heavier demands on computer resources in comparison with the real frequency equations.

IV. ENERGY SPECTRUM

The evolution of the hole spectral function with the concentration

$$x=-\frac{2}{\pi N}\sum_{\mathbf{k}}\int_{-\infty}^{\infty}d\omega n_F(\omega)\mathrm{Im}G(\mathbf{k}\omega)$$

is shown in Fig. 1 for different points of the Brillouin zone (all energy parameters here and in the following figures are given in units of t). A comparison of these results with the previous calculations,[4,5] where anomalous magnon Green's functions (3) were ignored, shows that they are unessential at small x and lead to some quantitative changes for moderate x (especially near the paramagnetic transition $x\approx 0.19$). The most essential, qualitatively, changes occur in the overdoped region $x\gtrsim 0.19$.

At $x\lesssim 0.04$ the spectra contain series of maxima corresponding to narrow spin-polaron bands [curves 1 in Fig. 1; energy vs momentum relationships for these bands are given in Fig. 3(a) of Ref. 5]. For larger x these peaks, excluding the lowest one, are washed away (curves 2 in Fig. 1). The dependence of the energies of the remaining peaks on $\mathbf{k}$ corresponds to a band with bandwidth of the order of t which is much larger than J, the characteristic width of the spin-polaron bands. The evolution of the hole energy spectrum with doping for $x>0.04$ is shown in Fig. 2. The portion of the arising wide energy band near the Fermi level in Fig. 2(a) and Fig. 2(b) originates from the lowest spin-polaron band and partly retains its dispersion. This portion corresponds to narrow intensive peaks of the spectral function and remains on or in the nearest vicinity of the Fermi level up to $x\approx 0.19$ (notice that the hole picture is used and states below the Fermi level are filled by holes). In Fig. 2(b) the shape of the hole band for moderate x is compared with the band $E_{\mathbf{k}}=2t[\cos(k_x)+\cos(k_y)]$ produced by the kinetic term of the t-J Hamiltonian at an utter absence of correlations (in the used magnetic Brillouin zone this latter band has two branches). An apparent similarity of the two bands indicates a certain weakening of correlations at $x>0.04$.

In parallel with the transformations in the hole spectrum changes occur in the magnon spectrum where the branch of overdamped magnons appear at $x\approx 0.02$ in the central part of the Brillouin zone.[3,4] The overdamped magnons manifest themselves in a perceptible intensity of the magnon spectral function $B_{11}(\mathbf{k}\omega)$ with a corresponding $\mathbf{k}$ at $\omega<0$. In this case the magnon occupation number $n_{\mathbf{k}}=-\int_{-\infty}^{\infty}(d\omega/\pi)n_B(\omega)B_{11}(\mathbf{k}\omega)$ is finite at $T=0$ which leads to a finite zero-temperature correlation length ξ in the correlation function

$$\langle S^z_{\mathbf{l}}S^z_{\mathbf{0}}\rangle\approx\left\{\frac{1}{2}-\frac{2}{N}\sum_{\mathbf{k}}[v^2_{\mathbf{k}}(1+n_{\mathbf{k}})+u^2_{\mathbf{k}}n_{\mathbf{k}}]\right\}^2+\left(\frac{2}{N}\right)^2\sum_{\mathbf{kk}'}e^{i\mathbf{l}(\mathbf{k}-\mathbf{k}')}u^2_{\mathbf{k}}v^2_{\mathbf{k}'}+\left(\frac{2}{N}\right)^2\sum_{\mathbf{kk}'}e^{i\mathbf{l}(\mathbf{k}-\mathbf{k}')}(u^2_{\mathbf{k}'}+v^2_{\mathbf{k}'})(u^2_{\mathbf{k}}+v^2_{\mathbf{k}})n_{\mathbf{k}},\quad(7)$$

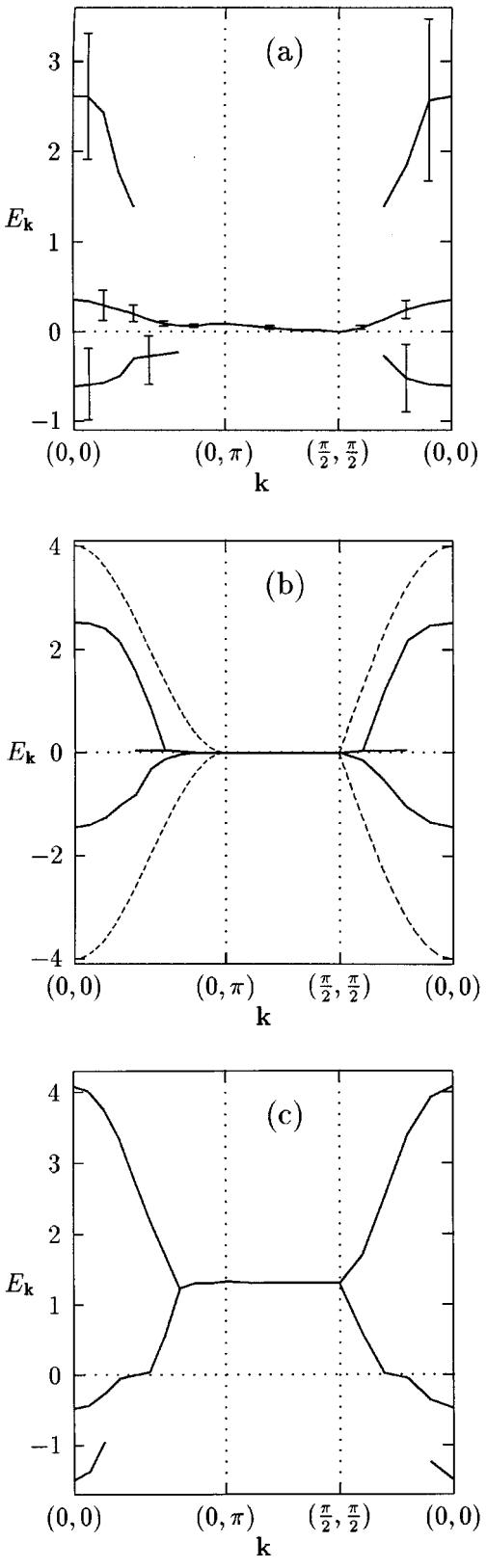

FIG. 2. Energy vs momentum relationships for $x=0.042$ (a), 0.169 (b), and 0.262 (c) (solid lines). $T=0$. Vertical bars in part (a) indicate halfwidths of the respective spectral peaks. For this x a weak peak, which can be associated with the second spin-polaron band, is observed between $\mathbf{k}=(0,0)$ and $(\pi/2,\pi/2)$. The respective dispersion curve is not shown in the figure. The dashed curve in part (b) is the band $E_{\mathbf{k}}=2t[\cos(k_x)+\cos(k_y)]$ in the magnetic Brillouin zone.

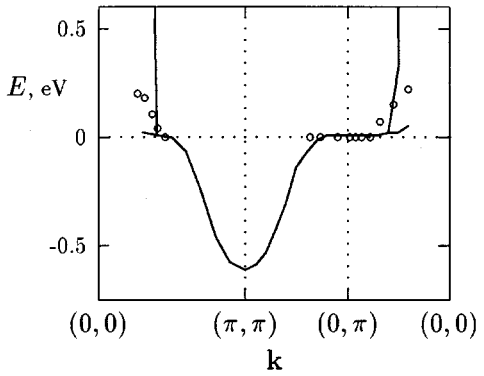

FIG. 3. The hole band obtained in the present calculations for $x=0.135$ (solid line). Circles indicate positions of quasiparticle peaks in the photoemission experiment in a Bi2212 crystal with $T_c=85$ K (from Ref. 1). Both the experimental and theoretical data correspond to $T=100$ K. The hole picture is used.

where $S_{\mathbf{l}}^z$ is the z component of the spin and sites $\mathbf{l}$ and $\mathbf{0}$ belong to the same sublattice. Thus, the mentioned changes in the magnon spectrum at $x\approx 0.02$ are connected with the destruction of long-range antiferromagnetic order and the establishment of short-range order. The size of the region in the Brillouin zone around the Γ point where the overdamped magnon branch is located and $n_{\mathbf{k}}\neq 0$ defines ξ. It can be shown[3] that in agreement with experiment[6] $\xi\approx 1/\sqrt{x}$ for small x. The critical concentration $x_c\approx 0.02$ is also close to the value observed[6,18] in $La_{2-x}(Ba,Sr)_xCuO_4$. The overdamped magnons can be identified with relaxational modes describing relative rotations of magnetic quantization axes in regions of size ξ. In the hole spectrum the destruction of long-range antiferromagnetic order manifests itself in the mentioned change of the characteristic energy of the spectrum from J to t at $x\approx 0.04$. Qualitatively this can be understood in the following way: In rigorous antiferromagnetic order the hole movement is accompanied by magnon emission and, as a consequence, the characteristic width of the hole bands coincides with the characteristic magnon energy J. After the destruction of long-range order holes can move without introducing additional disorder in the magnon subsystem and, as a result, the larger characteristic energy t reveals itself in the spectrum. Some additional details of the long-range to short-range antiferromagnetic transition and its manifestations in the hole and magnon spectra can be found in Refs. 3 and 4.

In Fig. 3 the hole band of the t-J model is compared with photoemission data of Ref. 1 from a Bi2212 crystal. Both experimental and theoretical data correspond to $T=100$ K ($T=0.017t$ for $t=0.5$ eV). In the experiment a crystal with $T_c=85$ K was used for which the hole concentration can be estimated to lie in the range $0.12\lesssim x\lesssim 0.16$. The value $x=0.135$ was taken for the calculations. Since for such x long-range antiferromagnetic order is already destroyed, the data are shown in the usual Brillouin zone, for which purpose some portions of the theoretical band are transferred from the first magnetic Brillouin zone to the second one [the

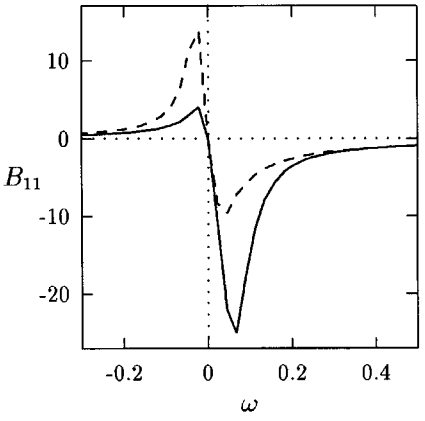

FIG. 4. The magnon spectral function $B_{11}(\mathbf{k}\omega)$ for $x=0.188$ (solid line) and 0.195 (dashed line). $\mathbf{k}=(\pi/2,\pi/2)$, $T=0$.

total shape of the band in Fig. 3 is similar to that shown in Fig. 2(b)]. The hole picture is used and hence the photoemission points are located on and above the Fermi level (to convert to the electron picture the data should be reflected at the Fermi level). In this comparison it is necessary to take into account the rapid increase of the decay widths of states with distance from the Fermi level [for the given concentration range these widths are comparable with those shown in Fig. 2(a)]. As a result, a higher-energy portion of the theoretical curve in Fig. 3 can be expected to be lost to a background observed in the experiment. Besides, extensions of the nearly dispersionless portion of the band near $E=0$ beyond the higher-energy branches correspond to weak maxima on a background of much more intensive maxima of these branches [see curve 2 in Fig. 1(c)]. With these remarks the quasiparticle dispersion of the t-J model can be concluded to be in satisfactory agreement with the experiment in Bi2212.

When $0.04\lesssim x\lesssim 0.19$ the hole energy band in the t-J model has large flat regions on and in the nearest vicinity of the Fermi level around the points $\mathbf{k}=(\pm\pi,0)$, $(0,\pm\pi)$ (at smaller x the respective regions of the spin-polaron band are far from the Fermi level). This result agrees with previous calculations.[4,5] As seen in Fig. 3, by the position and extension these regions are analogous to the extended saddle points observed in photoemission.[1] For the parameters of this figure the flat regions of the calculated band are positioned approximately 10 meV above the Fermi level, while the experimental value[1,19] is ± 30–50 meV for Bi2212 and 19 meV for $YBa_2Cu_4O_8$. Notice that the flat regions are shifted, in the absolute scale, to higher energies with growing x, remaining near the Fermi level up to $x\approx 0.19$. As expected[1,2] and confirmed by calculations,[5] they play the key role in the superconducting transition.

In comparison with transformations near $x=0.04$ even sharper changes of the spectral shapes proceed at $x\approx 0.19$. As follows from Fig. 1, sharp quasiparticle peaks jump from the periphery to the central part of the magnetic Brillouin zone. It should be emphasized that these changes occur in the narrow concentration range $x=0.188$–0.195. For the system considered the sharp quasiparticle peaks at the periphery of the magnetic Brillouin zone, which are observed in a wide range of concentrations starting from $x=0$, are the distinctive property of long- or short-range antiferromagnetic ordering. The jump of these peaks to the central part of the zone suggests the destruction of this ordering and the establishment of a completely disordered paramagnetic state.

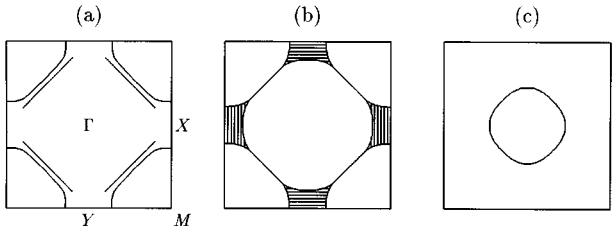

FIG. 5. The Fermi surface for $x=0.131$ (a), $x=0.188$ (b), and $x=0.316$ (c). Hatched regions in part (b) are the two-dimensional portions of the surface. In part (a), the points X, Y, and M correspond to $\mathbf{k}=(\pi,0)$, $(0,-\pi)$, and (π,π), respectively.

This conclusion is also supported by sharp changes in the magnon spectrum at $x\approx 0.19$ which are illustrated by Fig. 4. The domain of existence of the overdamped magnon branch around the Γ point grows with growing x and for $x\gtrsim 0.1$ the spin correlation length ξ is decreased to one to two lattice periods at $T=0$. In spite of this short correlation length, a peak corresponding to the usual magnon branch is well seen at $\omega>0$ up to $x=0.188$ (Fig. 4; the maximal magnon frequency at $\mathbf{k}=(\pi/2,\pi/2)$ is decreased[20,4] from the unperturbed value $2J$ with increasing x). However, already at $x=0.195$ this peak disappears and only the overdamped magnon is observed. For $x=0.195$ the real part of its frequency is less than the used frequency step and the spectral intensity is comparable on both sides of $\omega=0$. This result implies the complete destruction of the usual magnon branch and of the short-range antiferromagnetic ordering along with it.

A number of experimental results indicates that the transition from short-range antiferromagnetic order to a paramagnetic state really occurs in cuprates. The disappearance or a substantial weakening of magnetic correlations in the normal state of overdoped $YBa_2Cu_3O_{7-y}$, observed in neutron scattering experiments,[9] is direct evidence of such a transition. A radical change in the electronic state of overdoped crystals, which accompanies the transition, was detected in experiments[21] on the in-plane resistivity of Zn-substituted single crystals $YBa_2Cu_3O_{7-y}$ and $La_{2-x}Sr_xCuO_4$.

The applicability of the spin-wave approximation to the paramagnetic region of concentrations $x\gtrsim 0.19$ is subject to serious question. Nevertheless, some results obtained with model Hamiltonian (1) may be relevant to the considered system. With an increase of the hole concentration from the value $x\approx 0.19$ the shape of the hole energy band approaches the usual rigid 2D nearest-neighbor band [Fig. 2(c)]. The Fermi surface and the density of states $\rho(\omega)=-(2/\pi)\Sigma_{\mathbf{k}}\mathrm{Im}G(\mathbf{k}\omega)$ very accordingly, as shown in Figs. 5 and 6. The flat regions of the hole band determine the shape of the Fermi surface when $0.04\lesssim x\lesssim 0.19$. At $0.15\lesssim x\lesssim 0.19$ these regions are placed directly on the Fermi level and holes form an anomalous 2D Fermi liquid with a Fermi surface which is also two dimensional.[5] Representative shapes of the Fermi surface in the ranges of hole concentrations $0.04\lesssim x\lesssim 0.15$ and $0.15\lesssim x\lesssim 0.19$ are shown in

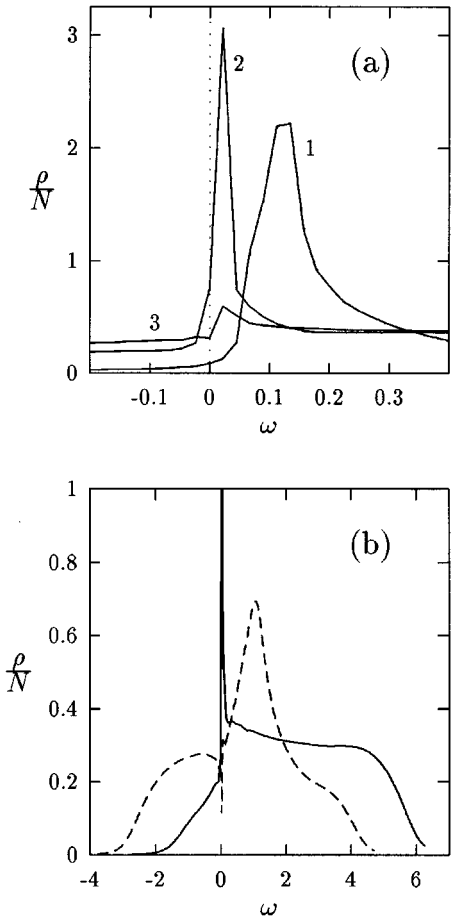

FIG. 6. The density of states in units of state/eV Cu spin near the Fermi level (a) and in a wider frequency range (b). $t=0.5$ eV . In part (a), curves 1, 2, and 3 correspond to $x=0.021$, 0.101, and 0.195, respectively. In part (b), the solid curve corresponds to $x=0.101$ the dashed curve to $x=0.316$, respectively.

Figs. 5(a) and 5(b). Analogous Fermi surfaces were observed in Bi2212 and Bi2201.[1] When x exceeds 0.19 the flat regions disappear and the Fermi surface acquires an ordinary form [Fig. 5(c)]. At $0.04\lesssim x\lesssim 0.19$ the flat regions produce a pronounced maximum in the density of states near the Fermi level (Fig. 6). Notice that the calculated maximal $\rho\approx 3$ state/eV Cu spin is close to experimental estimations[22] for Bi compounds. This maximum disappears when $x\gtrsim 0.19$ and the density of states approaches the shape of the usual 2D nearest-neighbor band [the dashed line in Fig. 6(b)].

V. SUPERCONDUCTIVITY

The strong-coupling Eliashberg formalism[23] and the obtained hole and magnon spectral functions were used for calculating T_c. Even- and odd-frequency order parameters belonging to all one-dimensional representations of the point group D_4 of the CuO_2 plane were tested for singlet pairing. In comparison with our previous consideration[5,24] the equation for the anomalous self-energy $\phi(\mathbf{k}\sigma,i\omega_n)$ contains new terms, connected with the anomalous magnon Green's functions. In the range of hole concentrations $x\lesssim 0.19$ these terms, however, do not alter the main conclusion of Refs. 5 and 24: The hole-magnon interaction is unable alone to give rise to superconductivity. The reason is a negligibly small coupling with magnons transferring holes from one portion of the Fermi surface to another which is eventually connected with spin flips accompanying the hole movement [see Eq. (1)]. Thus, in spite of the favorable condition for superconductivity — the large density of states near $\omega=0$, which is created by the hole-magnon interaction — it cannot make use of the condition itself.

However, the large density of states can be utilized by another hole-boson interaction, first of all by the interaction with full-symmetric apex oxygen vibrations which in accordance with the tunneling[25] and Raman[26] spectroscopy data interact most strongly with holes. The respective terms of the Hamiltonian originate from the zero-order, level-energy terms of the procedure[12] reducing the Emery Hamiltonian to the t-J Hamiltonian. Doped hole states are mainly constructed from four p orbitals of oxygens surrounding a copper site. Since two neighboring plaquettes contain a common oxygen site, there are two comparable terms in the hole-phonon interaction which describe changes in level energies with displacements of apex oxygen in the same and in the neighboring cells (a more detailed discussion see in Ref. 24):

$$H_{h\text{-ph}}=\sqrt{\frac{2}{N}}\sum_{\mathbf{k}\mathbf{k}'\sigma} h^{\dagger}_{\mathbf{k}\sigma}h_{\mathbf{k}'\sigma}(\sqrt{S_1\Omega}\,Q_{\mathbf{k}-\mathbf{k}',\sigma} + 4\gamma_{\mathbf{k}-\mathbf{k}'}\sqrt{S_2\Omega}\,Q_{\mathbf{k}-\mathbf{k}',-\sigma}), \tag{8}$$

where $Q_{\mathbf{k}\sigma}=\beta_{\mathbf{k}\sigma}+\beta^{\dagger}_{-\mathbf{k},\sigma}$ and $\beta^{\dagger}_{\mathbf{k}\sigma}$ is the creation operator of a phonon with the frequency Ω (a weak dispersion of relevant phonons is neglected). The Stokes shifts S_1 and S_2 characterize interactions of a hole with apex oxygen deformations in the same and in the neighboring cells, respectively. Notice that Hamiltonian (8) can also describe interactions of holes with in-plane and other interplane oxygen vibrations. It should be emphasized that the order of transformations leading to hole-phonon interaction (8) — first the reduction of the Emery Hamiltonian to the t-J Hamiltonian and then the introduction of the hole-phonon interaction — reflects the hierarchy of the relevant energy parameters: The Hubbard repulsion on copper[17] is much larger than the hole-phonon interaction constants S_1 and S_2.

The presence of two comparable terms in the Hamiltonian which describe the interaction of holes and phonons in different sublattices is essential for singlet superconductivity on the antiferromagnetic background. Only the interference of these terms contributes to singlet pairing, as holes with different spins move within different sublattices.

For Hamiltonians (1) and (8) the linearized equation for the anomalous self-energy can be written in the form

$$\phi(\mathbf{k}\sigma,i\omega_n)=2T\sum_{\mathbf{q}m}\Big[2g_{\mathbf{k},\mathbf{k}+\mathbf{q}}g_{\mathbf{q},\mathbf{k}+\mathbf{q}}\mathrm{Re}D_{11}(\mathbf{k}+\mathbf{q},i\omega_n+i\omega_m) + g^2_{\mathbf{k},\mathbf{k}+\mathbf{q}}D_{12}(\mathbf{k}+\mathbf{q},i\omega_n+i\omega_m) + g^2_{\mathbf{q},\mathbf{k}+\mathbf{q}}D_{21}(\mathbf{k}+\mathbf{q},i\omega_n+i\omega_m) + \frac{4\varepsilon}{N}\gamma_{\mathbf{k}-\mathbf{q}}-\frac{8S\Omega}{N}\gamma_{\mathbf{k}-\mathbf{q}}C(\mathbf{q}-\mathbf{k},i\omega_m-i\omega_n)\Big] \times|G(\mathbf{q},i\omega_m)|^2\phi(\mathbf{q}\sigma,i\omega_m), \tag{9}$$

where $S=\sqrt{S_1 S_2}$ and the phonon Green's function $C(\mathbf{k},i\omega_\nu)$ is the Fourier transform of

$$C(\mathbf{k}\tau)=-\langle \mathcal{T}Q_{\mathbf{k}\sigma}(\tau)Q^{\dagger}_{\mathbf{k}\sigma}\rangle.$$

The anomalous self-energy in Eq. (9) can be described by the following diagrams:

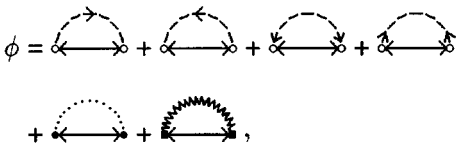

where solid and dashed lines correspond to hole and magnon Green's functions, the dotted line to the hole-hole interaction, and the wavy line to the phonon Green's function, respectively.

In subsequent calculations comparatively small changes in the phonon spectrum, caused by the hole-phonon interaction,[26] are neglected and $C(\mathbf{k},i\omega_\nu)$ is substituted by the unperturbed value $-2\Omega/(\Omega^2+\omega_\nu^2)$. For the considered moderate hole-phonon interaction hole and magnon energy spectra are mainly determined by the hole-magnon interaction.[27] Therefore in Eq. (9) we use hole and magnon Green's functions from the previous section, neglecting the influence of the hole-phonon interaction on them. Although in Eq. (9) Green's functions do not depend on σ, $\phi(\mathbf{k}\sigma,i\omega_n)$ may change sign with σ to satisfy the condition $\phi(\mathbf{k}\sigma,i\omega_n)=-\phi(-\mathbf{k},-\sigma,-i\omega_n)$ following from the definition of the anomalous hole Green's function.

In addition to parameters (6), in solving Eq. (9) the phonon frequency Ω was taken to be $0.15t$. This value is approximately equal to the frequency of the full-symmetric apex oxygen vibrations in Bi2212.[26] The hole-phonon interaction constant $S=1.2t$ was selected, which provides T_c lying in the range observed in cuprates. This value of S corresponds to a moderate dimensionless coupling constant $\lambda\sim S/B$, where $B\approx 3t-5t$ is the hole bandwidth at $x\gtrsim 0.04$. In solving Eq. (9) the infinite summation over m has been substituted by a finite one with the cutoff $|\omega_m|\leqslant 20J$, which has been proved to have no effect on results in the considered temperature range.

Equation (9) can be considered as an eigenvalue equation for the vector $\phi(\mathbf{k}\sigma,i\omega_n)$.[23] The order parameter becomes nonzero and $T=T_c$ when the largest eigenvalue becomes equal to one. At $S=0$ and $x\lesssim 0.19$ the largest, but less than 1, eigenvalue of Eq. (9) corresponds to an even-frequency $d_{x^2-y^2}$ solution (see Fig. 7). This symmetry of the leading solution was found in a large number of works considering an interaction with antiferromagnetic fluctuations as the main mechanism for pairing.[10] For $x\lesssim 0.19$ in our calculations the superconducting transition was found to occur only with the incorporation of the hole-phonon interaction. As seen in Fig. 8, in the considered model high values of T_c are already attained at moderate hole-phonon coupling for the even-frequency $d_{x^2-y^2}$ pairing. This is connected with the fact that, like the hole-magnon interaction, the hole-phonon interaction (8) favors this type of pairing. As a consequence, for this symmetry there is no competition between the two interactions, in contrast with other considered symmetries where eigenvalues grow only slightly with the incorporation of the hole-phonon interaction. The second reason for high T_c's is the large maximum of the density of states near the Fermi level. As follows from Fig. 8, T_c rapidly drops when the maximum moves away from the Fermi level ($x\lesssim 0.04$) or is destroyed ($x\gtrsim 0.19$). The third reason for high T_c's is high frequencies of relevant oxygen vibrations in cuprates.[26] These frequencies exceed significantly phonon frequencies in conventional superconductors.

Results shown in Fig. 8 differ somewhat from those obtained in Ref. 5 for the range $x\lesssim 0.19$. This difference is mainly connected with changes introduced by the anomalous magnon Green's functions into spectral functions near the paramagnetic transition. Another source of the difference is the use of retarded Green's functions calculated for a respective temperature in Eq. (9). In Ref. 5 Matsubara Green's functions in the equation for the anomalous self-energy were calculated from zero-temperature retarded Green's functions.

Only the on-site part of the Coulomb repulsion was taken into account in the above consideration. The long-range part of this repulsion and phase fluctuations,[28] which are out of scope of the mean-field Eliashberg theory, will substantially decrease T_c in the region of small x near $x=0.04$.

As follows from Fig. 7, after the destruction of short-range antiferromagnetic order at $x\approx 0.19$ the even-frequency

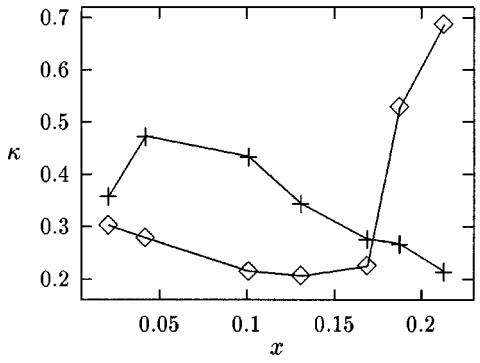

FIG. 7. Eigenvalues κ of the leading solutions of Eq. (9): an even-frequency $d_{x^2-y^2}$ solution (+) and odd-frequency s solution ($\diamond$). $S=0$ and $T=0.01t$. Connecting lines are for guiding the eye only.

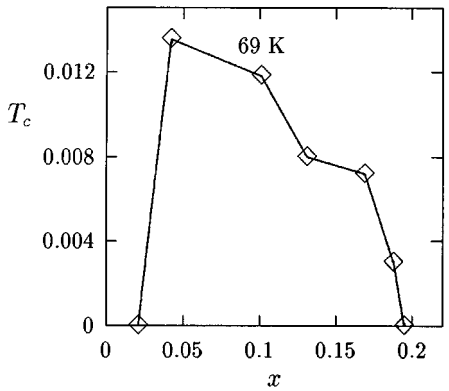

FIG. 8. T_c vs x for the even-frequency $d_{x^2-y^2}$ gap, parameters (6), $\Omega=0.15t$, and $S=1.2t$. T_c is recalculated in kelvin for $t=0.5$ eV. Connecting lines are for guiding the eye only.

$d_{x^2-y^2}$ solution ceases to be the leading solution of Eq. (9) with $S=0$. For $x \gtrsim 0.19$ the odd-frequency s solution becomes the leading one. At fixed temperature its eigenvalue rapidly growth with x and even runs to unity between $x=0.262$ and 0.316 which is an indication of the superconducting transition. As indicated, the applicability of the spin-wave approximation to the paramagnetic region of concentrations is subject to serious question and it is unlikely that this result may have any bearing on cuprates. However, it should be noted that the eigenvalue starts to grow already at $x<0.19$ and attains a large magnitude there. This means that the incorporation of a hole-phonon interaction of the appropriate symmetry would lead to superconductivity with odd-frequency s-wave pairing near the boundary $x \approx 0.19$. The hole-phonon interaction of the required symmetry may be obtained from the first-order hopping term of the procedure[12] reducing the Emery Hamiltonian to the t-J Hamiltonian. Thus, according to our calculations the even-frequency $d_{x^2-y^2}$-wave superconductivity would be expected for underdoped and optimally doped crystals ($x \lesssim 0.19$) and odd-frequency s-wave superconductivity, for overdoped crystals. Different experiments designed to probe the symmetry of the superconducting state give contradictory results which can be interpreted as $d_{x^2-y^2}$, s, or mixed type of symmetry.[10,29] In this connection it would be of particular interest to use samples with different and controllable concentrations of holes in these experiments.

In summary, the spin-wave and Born approximations were used for self-consistent calculations of the energy spectrum of the t-J model in the range of hole concentrations $0 \leqslant x \lesssim 0.3$. The hole and magnon spectra undergo two sharp transformations at $x \approx 0.02$–0.04 and 0.19 which are connected with the transitions from long-range to short-range antiferromagnetic order and from short-range order to a completely disordered paramagnetic state. For $0.04 \lesssim x \lesssim 0.19$ the shape of the Fermi surface, the hole dispersion near the Fermi level, and the density of states on it are in satisfactory agreement with experiment in $La_{2-x}Sr_xCuO_4$ and Bi2212. The Eliashberg formalism was used for calculating T_c. The hole-magnon interaction was found to be unable alone to give rise to superconductivity. By adding a moderate interaction with apex oxygen vibrations high T_c's were obtained for even-frequency $d_{x^2-y^2}$ pairing in the range $0.04 \lesssim x \lesssim 0.19$. For larger hole concentrations the odd-frequency s-wave solution was found to have the largest eigenvalue which creates conditions for the s-wave superconductivity in the overdoped regime.

ACKNOWLEDGMENTS

This work was partially supported by the Estonian Science Foundation under Grant No. ETF-67 and by a WTZ grant (Project No. EST112.1) of the BMBF.

[1] Z.-X. Shen and D. S. Dessau, Phys. Rep. **253**, 1 (1995).
[2] D. M. Newns, H. R. Krishnamurthy, P. C. Pattnaik, C. C. Tsuei, C. C. Chi, and C. L. Kane, Physica B **186-188**, 801 (1993).
[3] A. Sherman and M. Schreiber, Phys. Rev. B **48**, 7492 (1993).
[4] A. Sherman and M. Schreiber, Phys. Rev. B **50**, 12 887 (1994).
[5] A. Sherman and M. Schreiber, Physica C **253**, 23 (1995).
[6] B. Keimer, N. Belk, R. G. Birgeneau, A. Cassanho, C. Y. Chen, M. Greven, M. A. Kastner, A. Aharony, Y. Endoh, R. W. Erwin, and G. Shirane, Phys. Rev. B **46**, 14 034 (1992).
[7] S. Schmitt-Rink, C. M. Varma, and A. E. Ruckenstein, Phys. Rev. Lett. **60**, 2793 (1988); C. L. Kane, P. A. Lee, and N. Read, Phys. Rev. B **39**, 6880 (1989).
[8] A. V. Sherman, Physica C **171**, 395 (1990).
[9] L. P. Regnault, P. Bourges, P. Burlet, J. Y. Henry, J. Rossat-Mignod, Y. Sidis, and C. Vettier, Physica C **235-240**, 59 (1994); Hung Fai Fong, B. Keimer, P. W. Anderson, D. Reznik, F. Doğan, and I. A. Aksay, Phys. Rev. Lett. **75**, 316 (1995).
[10] J. R. Schrieffer, Solid State Commun. **92**, 129 (1994).
[11] F. C. Zhang and T. M. Rice, Phys. Rev. B **37**, 3759 (1988).
[12] A. V. Sherman, Phys. Rev. B **47**, 11 521 (1993); Physica C **211**, 329 (1993).
[13] V. J. Emery, Phys. Rev. Lett. **58**, 2794 (1987).
[14] J. E. Hirsch, Phys. Rev. Lett. **59**, 228 (1987).
[15] A. B. Migdal, Zh. Eksp. Teor. Fiz. **34**, 1438 (1958) [Sov. Phys. JETP **7**, 996 (1958)].
[16] N. M. Plakida, P. Horsch, A. Liechtenstein, and V. S. Oudovenko (unpublished).
[17] A. K. McMahan, J. F. Annett, and R. M. Martin, Phys. Rev. B **42**, 6268 (1990).
[18] G. Aeppli, S. M. Hayden, H. A. Mook, T. E. Mason, A. D. Taylor, K. N. Clausen, T. G. Perring, S.-W. Cheong, Z. Fisk, and D. Rytz, Physica B **192**, 103 (1993).
[19] K. Gofron, J. C. Campuzano, A. A. Abrikosov, M. Lindroos, A. Bansil, H. Ding, D. Koelling, and B. Dabrowski, Phys. Rev. Lett. **73**, 3302 (1994).
[20] J. Igarashi and P. Fulde, Phys. Rev. B **45**, 12357 (1992); G. Khaliullin and P. Horsch, *ibid*. **47**, 463 (1993); G. Krier and G. Meissner, Ann. Phys. **2**, 738 (1993).
[21] Y. Fukuzumi, K. Mizuhashi, K. Takenaka, and S. Uchida, Phys. Rev. Lett. **76**, 684 (1996).
[22] J. B. Torrance, A. Bezinge, A. I. Nazzal, and S. S. P. Parkin, Physica C **162-164**, 291 (1989); P. Mandal, A. Poddar, B. Ghosh, and P. Choudhury, Phys. Rev. B **43**, 13 102 (1991).
[23] G. M. Eliashberg, Zh. Eksp. Teor. Fiz. **38**, 966 (1960) [Sov. Phys. JETP **11**, 696 (1960)]; P. B. Allen and B. Mitrović, Solid State Phys. **37**, 1 (1982).
[24] A. Sherman and M. Schreiber, Phys. Rev. B **52**, 10 621 (1995).
[25] S. I. Vedeneev and V. I. Stepanov, Pis'ma Zh. Eksp. Teor. Fiz. **49**, 510 (1989) [JETP Lett. **49**, 588 (1989)].
[26] Yu. E. Kitaev, M. F. Limonov, A. P. Mirgorodskii, A. G. Panfilov, and R. A. Evarestov, Fiz. Tverd. Tela **36**, 865 (1994) [Sov. Phys. Solid State **36**, 475 (1994)].
[27] J. Sabczynski, A. Sherman, and M. Schreiber, Phys. Lett. A **195**, 231 (1994).
[28] V. J. Emery and S. A. Kivelson, Nature **374**, 434 (1995).
[29] R. C. Dynes, Solid State Commun. **92**, 53 (1994).